Mixed mode oscillations and phase locking in coupled FitzHugh-Nagumo model neurons

Cite as: Chaos **29**, 033105 (2019); doi: 10.1063/1.5050178
Submitted: 27 July 2018 · Accepted: 8 February 2019 ·
Published Online: 1 March 2019

Elizabeth N. Davison,[1,a)] Zahra Aminzare,[2] Biswadip Dey,[1] and Naomi Ehrich Leonard[1]

AFFILIATIONS

[1]Department of Mechanical and Aerospace Engineering, Princeton University, Princeton, New Jersey 08540, USA
[2]Department of Mathematics, University of Iowa, Iowa City, Iowa 52242, USA

[a)]**Electronic mail:** end@princeton.edu

ABSTRACT

We study the dynamics of a low-dimensional system of coupled model neurons as a step towards understanding the vastly complex network of neurons in the brain. We analyze the bifurcation structure of a system of two model neurons with unidirectional coupling as a function of two physiologically relevant parameters: the external current input only to the first neuron and the strength of the coupling from the first to the second neuron. Leveraging a timescale separation, we prove necessary conditions for multiple timescale phenomena observed in the coupled system, including canard solutions and mixed mode oscillations. For a larger network of model neurons, we present a sufficient condition for phase locking when external inputs are heterogeneous. Finally, we generalize our results to directed trees of model neurons with heterogeneous inputs.

Efforts to gain insight into the complex dynamics of the brain benefit from a detailed understanding of neurons and their interactive dynamics. We study a system of two model neurons where the first neuron receives a constant external input and the second neuron receives an input from the first neuron. Systems of two coupled model neurons exhibit rich dynamical patterns that can represent large networks comprised of two distinct clusters. This makes them fascinating in their own right and useful as a starting point for studying more general networks. Using the bifurcation theory, we find bounds on the external input and coupling strength that predict firing, mixed mode oscillations, and phase locking. We extend these conditions to more general networks. Our results provide foundations for investigating the interplay between structure and external stimuli in networks of neurons.

I. INTRODUCTION

The study of model neurons has a rich history, dating back to the pioneering work of Hodgkin and Huxley[1] on the action potential in the squid giant axon. A two-dimensional model that captures salient qualities of the four-dimensional Hodgkin-Huxley model was developed independently by FitzHugh[2,3] and Nagumo *et al.*[4] In this model, commonly known as the FitzHugh-Nagumo (FN) model, one variable represents the membrane potential and the other represents a gating variable. A constant external input to the FN model neuron can produce quiescent behavior (a low-voltage stable equilibrium point), firing (a stable limit cycle), or saturated behavior (a high-voltage stable equilibrium point). The FN model neuron captures realistic neuronal behavior such as spike accommodation, bistability, and excitability.[5]

A system of two coupled neurons can represent a larger network of neurons that cluster into two groups in which neurons within each group synchronize but neurons in different groups do not. A cluster synchronized network can be reduced to a *quotient network*[6,7] by leveraging balanced conditions on coupling and graph structure,[8] as well as bounds on coupling strength.[9,10] A system of two FN model neurons with gap junction diffusive coupling (two-FN system) has been studied numerically and analytically in the symmetric case,[11,12] where both neurons receive the same external input and are coupled bidirectionally (undirected coupling). Gap junction diffusive coupling is modeled as a difference between the membrane potentials of the two model neurons multiplied by a parameter that represents the coupling strength. The two-FN system has also been studied numerically[11] in a context where the intrinsic properties of both models are the same but the neurons are coupled unidirectionally (directed coupling). Here, we add to the existing literature by

analytically describing the bifurcation structure of the directed two-FN system in terms of two parameters, the external input to the first model neuron and the unidirectional coupling strength from the first model neuron to the second.

The FN model neuron is a classic example of a fast-slow system, and the coupled pair of FN model neurons exhibit rich dynamics characterized by the timescale separation. Under certain conditions on external input and coupling strength, the system exhibits *canard solutions*, which are solutions that pass from a stable to an unstable manifold in the slow system and stay near the unstable manifold for a long time relative to the slow system timescale.[13–15] Canard solutions result from the presence of two distinct types of folded singularities, stable folded nodes, and folded saddles. In particular, stable folded nodes give rise to robust families of canard solutions.[14,16] When combined with a suitable return mechanism, canard solutions can lead to mixed mode oscillations (MMOs), which are periodic oscillations that alternate between canard-driven oscillations and a relaxation oscillation.[17] The existence of canards and MMOs has been described for systems in four dimensions,[14,18] systems with two slow variables and two fast variables,[19] and generalized systems in arbitrary finite dimensions.[20] The folded saddle node of type I (FSN I) and folded saddle node of type II (FSN II) have been identified as mechanisms for the onset of MMOs in fast-slow systems.[17,21–24] We leverage these results to determine the regions of parameter space where canards and MMOs may be present in the directed two-FN system, which has two slow variables and two fast variables.

Canard-induced MMOs have been studied analytically in numerous systems including chemical reactions,[25,26] the Hodgkin-Huxley neuronal model,[27] cortical grid cells,[28] and a self-coupled FN model neuron.[29] In a two-FN system, the onset of firing, as coupling strength is increased, can be characterized by the appearance of canard solutions and by MMOs, as the coupling is increased further. The existence of canard solutions in a two-FN system was first proven using nonstandard analysis in the case of model neurons with identical parameters.[30] Necessary conditions were found in terms of a model parameter that controls the slope of the linear nullcline of the system. Conditions for different stability types of folded singularities were found in terms of the same model parameter in a slightly modified, but still symmetric, model.[31] Here, we fix the corresponding parameter within the range where canard solutions may be present and find conditions for the existence of canard-induced MMOs in terms of two parameters that break symmetry: external input and coupling strength.

A condition for the onset of MMOs in a two-FN system was shown as an application of a method developed to study MMOs in systems with two fast variables and two slow variables.[32] There are no symmetry requirements and the main result is a necessary condition for the MMO onset in terms of a parameter corresponding to the input to one of the neurons. In the spirit of this work, we prove explicit necessary conditions for existence of canard solutions and MMOs in the directed two-FN system in terms of both the external input and the coupling strength. First, we take the singular limit of the system, and obtain necessary conditions on the bifurcation parameters for existence of transcritical bifurcations. The transcritical bifurcations in the singularly perturbed system delineate regions in parameter space where MMOs exist in the original system.

We show, further, that the original system admits Hopf bifurcations within a distance of order ϵ around the point in the parameter space where the singularly perturbed system admits transcritical bifurcations. This we use to derive novel bounds for phase-locking in representative networks of model neurons. Phase locking is a generalization of synchronization where the phases of oscillating models remain separated by a constant offset, while amplitudes and waveforms may vary.[33] A common phenomenon in nature, phase locking has been studied in cardiac rhythms,[34–36] in the firing patterns of squid axons,[37] in two coupled phase oscillators,[38] in local field potential measurements of neurons in the human brain,[39,40] and in the brain as a mechanism for coordination between groups of neurons.[41]

Finally, we consider the more general problem of n FN model neurons linked by unidirectional gap junction diffusive coupling in a directed tree, with heterogeneous coupling strengths and heterogeneous external inputs. As in the directed two-FN system, this can represent a class of large networks that contain cluster synchronized groups of model neurons and satisfy conditions on graph structure[8] and connectivity[9,10] so they can be reduced to a quotient network.[6,7] An analogous problem with homogeneous coupling strength has been analyzed in detail in the strong coupling limit where the dynamics are reduced using the singular perturbation theory.[42] Here, we leverage an analysis of the singular perturbation of the directed two-FN system to provide necessary conditions for the existence of MMOs and sufficient conditions for phase locking in the original n-FN system.

Our contributions towards understanding the dynamics of networked nonlinear model neurons are as follows. First, we explain how the bifurcation structure of the directed two-FN system relates to the bifurcation structure of the reduced, singularly perturbed system that is used to study canard solutions. This is critical because the reduced system can be used to explain features of the original system and the original system can be used to understand the reduced system. Second, we provide necessary conditions for canards and MMOs in the directed two-FN system in terms of two model parameters; this is an extension of the conditions found in terms of one parameter in the literature. Third, we provide a sufficient condition for phase locking given heterogeneous external inputs in the directed two-FN system. We generalize these conditions to directed trees of FN model neurons.

The paper is organized as follows. In Sec. II, we review the standard analysis of a single FN model neuron and give a biophysical rationale for bounds on model parameters used throughout the paper. In Sec. III, we define the directed two-FN system and find conditions for Hopf bifurcations. In Sec. IV, we compute the singular perturbation of the directed two-FN system. We prove necessary conditions for the transcritical bifurcations in the singularly perturbed system and canards and MMOs in the original system in Sec. V. In Sec. VI, we generalize the results to directed trees of FN model neurons. We provide a numerical example to illustrate our results.

II. SINGLE FITZHUGH-NAGUMO MODEL NEURON

The FN model is a two-dimensional simplification of the four-dimensional Hodgkin-Huxley (HH) model that retains conceptually relevant properties of the activation and deactivation dynamics of the

neuronal action potential. By letting y and z represent the membrane potential and a slow gating variable, respectively, its dynamics are given by

$$\begin{aligned} \frac{dy}{dt} &= \psi(y) - z + I, \\ \frac{dz}{dt} &= \epsilon(y - bz), \end{aligned} \tag{1}$$

where $\psi(y)$ is a cubic polynomial. For our purposes, we use $\psi(y) = y - \frac{y^3}{3} - a$. In this model, I corresponds to an external input, $0 < \epsilon \ll 1$ is a positive timescale separation constant, and a and b are positive constants.

The FN model is far simpler to analyze than the full HH model due to the lower dimension. Despite the lower dimension, the FN model captures key characteristics of the HH model and a range of physiologically meaningful regimes and behaviors.[5,43] The FN model is a suitable choice for network analysis because it is both dynamically rich and analytically tractable.

Hopf bifurcations are distinguishing features of the FN model dynamics. A *Hopf bifurcation* occurs when the variation in a parameter leads to the appearance or disappearance of an isolated limit cycle from an equilibrium point and a simultaneous change in stability of the equilibrium inside the limit cycle. In a *supercritical Hopf bifurcation*, the limit cycle is stable, while in a *subcritical Hopf bifurcation*, the limit cycle is unstable.

A necessary condition[44] for the FN model to exhibit distinct quiescent, firing, and saturated regimes is the existence of a unique equilibrium point for all values of the bifurcation parameter I. In this paper, we assume the following:

Assumption II.1. *Parameters a, b, and ϵ are such that the FN model (1) has a unique equilibrium point for all values of $I \geq 0$. This results in conditions $0 < a < 1$ and $0 < b < 1$.*

The condition on a corresponds to a simple voltage offset requirement and the condition on b corresponds to a requirement that the slope of the linear nullcline of (1) must be greater than that of the cubic nullcline of (1).

By Assumption II.1, there is one equilibrium point for all values of I. There are six key features in the bifurcation structure of the FN model as the external input parameter, I, is varied:

- $I = I_{0sn}$: As I is increased from zero, stable and unstable limit cycles appear through a saddle node bifurcation of limit cycles at $I = I_{0sn}$ for some $I_{0sn} > 0$, while the unique equilibrium point is stable. The large limit cycles are relaxation oscillations. The bifurcation at I_{0sn} defines the beginning of the firing regime and the small region of bistability.
- $I = I_{0c}$: As I is increased slightly, through the point $I = I_{0c}$,[45,46] there is a region of bistability during which there occurs a *canard explosion*, which is an abrupt transition from small limit cycle oscillations to larger limit cycle oscillations. The unique equilibrium point is still stable. By Ref. 47, the saddle node of limit cycles and the canard explosion occur at essentially the same parameter value, i.e., $I_{0c} \approx I_{0sn}$. We calculate an approximation to I_{0c} later in this section.
- $I = I_0$: As I is increased further, through a subcritical Hopf bifurcation at $I = I_0$, where $I_0 > I_{0c}$, the unstable limit cycles disappear, the stable equilibrium point becomes unstable, and the large stable limit cycles remain. The bifurcation at I_0 defines the end of the small region of bistability.
- $I = I_1$: For $I_0 < I < I_1$, for some $I_1 > 0$, there are only an unstable equilibrium point and the large stable limit cycle oscillations. At $I = I_1$, through another subcritical Hopf bifurcation, the equilibrium becomes stable and small unstable limit cycles appear. The bifurcation at I_1 defines the beginning of a second small region of bistability.
- $I = I_{1c}$: For $I_1 < I < I_{1c}$, the equilibrium is stable and there is again a region of bistability characterized by a canard explosion with the unique equilibrium point stable.[45,46] We calculate an approximation to I_{1c} later in this section.
- $I = I_{1sn}$: As I is increased slightly, through the point $I = I_{1sn}$, there is another saddle node bifurcation of limit cycles. The bifurcation at I_{1sn} defines the end of the firing regime and the second small region of bistability. By Ref. 47, the saddle node of limit cycles and the canard explosion occur at essentially the same parameter value, i.e., $I_{1sn} \approx I_{1c}$.

Figure 1 depicts the bifurcation diagram of the FN model when I is varied.

The following proposition from Ref. 46 describes the stability of the unique equilibrium point of (1) given Assumption II.1 and conditions on I for Hopf bifurcations.

Proposition II.2 (Ref. 46)**.** *Let Assumption II.1 hold. Then, there exists $I_0 < I_1$ such that the equilibrium point is stable for $I < I_0$ and, as I increases, it will undergo a transition to an unstable equilibrium point through a Hopf bifurcation at I_0. As I is increased further it will undergo a transition from unstable to stable through a second Hopf bifurcation at I_1.*

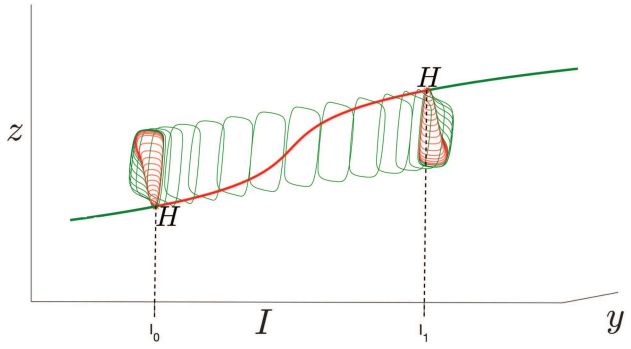

FIG. 1. Bifurcation diagram for a single FN model drawn with a numerical continuation software tool[48] for $a = 0.875$, $b = 0.8$, and $\epsilon = 0.08$. Green corresponds to stable equilibrium points or limit cycles, and red corresponds to unstable equilibrium points or limit cycles. For most values $I < I_0$, the FN model is in the quiescent regime. For $I_{0sn} \approx I_{0c} < I < I_0$, the FN model is in the firing regime since it concurrently exhibits a stable equilibrium point, small unstable oscillations, and larger stable oscillations. The FN model is always in the firing regime when $I_0 < I < I_1$. For $I_1 < I < I_{1c} \approx I_{1sn}$, the FN model is also in the firing regime since it concurrently exhibits a stable equilibrium point, small unstable oscillations, and larger stable oscillations. For all other $I > I_1$, the FN model is in the saturated regime.

We review the approach to analyzing stability of the limit cycles arising from the Hopf bifurcations following the methods of Chapter 3 of Ref. 46 and the application to the FN model in Ref. 49. We generalize the approach to networks of FN model neurons in Secs. III–VII.

The dynamics at a Hopf bifurcation at the origin of a two-dimensional system can be written as

$$\begin{pmatrix} \frac{dx_1}{dt} \\ \frac{dx_2}{dt} \end{pmatrix} = \begin{pmatrix} 0 & -\omega \\ \omega & 0 \end{pmatrix} \begin{pmatrix} x_1 \\ x_2 \end{pmatrix} + \begin{pmatrix} F(x_1, x_2) \\ G(x_1, x_2) \end{pmatrix} \tag{2}$$

such that F and G satisfy $F(0,0) = G(0,0) = 0$ and $D_{\mathbf{x}}F(0,0) = D_{\mathbf{x}}G(0,0) = \mathbf{0}$, where $D_{\mathbf{x}}F$ is the Jacobian of F with respect to $\mathbf{x}$ and $\mathbf{x} = (x_1, x_2)^\top$.

Definition II.3 (Cubic coefficient[46,50]). *Consider the system (2). The coefficient of the cubic term of the Taylor expansion of the RHS of (2) is expressed as*

$$\begin{aligned} \alpha = {} & \frac{1}{16}(F_{x_1x_1x_1} + F_{x_1x_2x_2} + G_{x_1x_1x_2} + G_{x_2x_2x_2})\Big|_{(0,0)} \\ & + \frac{1}{16\omega}(F_{x_1x_2}(F_{x_1x_1} + F_{x_2x_2}) - G_{x_1x_2}(G_{x_1x_1} + G_{x_2x_2}) \\ & - F_{x_1x_1}G_{x_1x_1} + F_{x_2x_2}G_{x_2x_2})\Big|_{(0,0)}, \end{aligned} \tag{3}$$

where $F_{x_1x_2}$ denotes $\dfrac{\partial^2 F}{\partial x_1 \partial x_2}$ and so on.

Proposition II.4 [Theorem 3.4.2 (modified)[46]]. *The system $\dot{\boldsymbol{x}} = \mathbf{f}(\mathbf{x}, \mu)$ admits a Hopf bifurcation for the parameter value $\mu = \mu_0$ at an equilibrium point $\mathbf{x} = \boldsymbol{0}$ if*

1. *$D_{\mathbf{x}}\mathbf{f}(\boldsymbol{0}, \mu_0)$ has a pair of pure imaginary eigenvalues and no other eigenvalues with zero real parts.*
2. *$\dfrac{\partial}{\partial \mu}\Re[\lambda(\mu)]\Big|_{\mu=\mu_0} \neq 0$, where $\Re(\lambda)$ denotes the real part of the eigenvalue λ.*
3. *The cubic coefficient of the Taylor expansion of $\mathbf{f}$, denoted by α and defined in Definition II.3, is nonzero.*

Furthermore, if $\alpha < 0$, the Hopf bifurcation is supercritical, while, if $\alpha > 0$, the Hopf bifurcation is subcritical.

The cubic coefficient is also called the first Lyapunov coefficient. For the FN model, the cubic coefficient is given by

$$\alpha = \frac{1}{8}\left(\frac{2b - b^2\epsilon - 1}{1 - b^2\epsilon}\right).$$

In this paper, we choose parameters that ensure Assumption II.1 holds and the bifurcations are subcritical Hopf ($\alpha > 0$); these yield biologically realistic dynamics.[51,52] We fix $a = 0.875$, $b = 0.8$, and $\epsilon = 0.08$, and we consider $I \geq 0$ as a bifurcation parameter.

The value of the bifurcation parameter I where canards exist near each Hopf bifurcation is close to the respective saddle node bifurcation of limit cycles and can be found following Ref. 53. Let $\mathbf{f}$ represent the dynamics of (1), and let F and G be defined as in (2) for (1), where $x_1 = y$ and $x_2 = z$. Following Eq. (3.23) of Ref. 53, we compute

$$I_{ic} = I_i - 8\,\frac{a_1}{F_{xx}\delta_i}\,\epsilon + \mathcal{O}(\epsilon^2), \quad i = 0, 1,$$

where I_i is the value of I at the Hopf bifurcation,

$$a_1 = \frac{1}{16}[F_{yy}(F_zG_{yy} - F_{yy}G_z) + G_y(F_{yz}F_{yy} - F_zF_{yyy})]$$

and

$$\delta_i = \frac{\partial}{\partial I}\{\mathrm{Tr}[D_{\mathbf{x}}\mathbf{f}(\mathbf{p}, I)]\}\Big|_{I=I_i}.$$

For the FN model (1), $I_{0c} = I_0 - 0.09\epsilon + \mathcal{O}(\epsilon^2)$ and $I_{1c} = I_1 + 0.09\epsilon + \mathcal{O}(\epsilon^2)$. So canards exists for $I_{0c} < I < I_0$ and for $I_1 < I < I_{1c}$, as illustrated in Fig. 1.

III. DIRECTED TWO-FN MODEL NEURON SYSTEM

The directed two-FN model neuron system is shown in Fig. 2. The first model neuron is denoted as A and it receives external input I. The second model neuron is denoted B and it receives no external input. The coupling is unidirectional from A to B, with coupling strength γ. A and B have the same intrinsic dynamics, i.e., the same values of a, b, and ϵ as defined above. We let I and γ be bifurcation parameters.

The two-FN system can be used to study cluster synchronized graphs containing two clusters. In this case, the dynamics can be reduced to a simplified quotient graph.[7,54] When there are many more model neurons in one cluster than the other, the coupling from the large cluster to the small cluster is much stronger than the coupling from the small cluster to the large cluster. Thus, we can disregard the coupling from the small cluster to the large cluster and the simplified graph can be approximated by the directed two-FN system.

The equations for the directed two-FN system are

$$\begin{aligned} \frac{dy_A}{dt} &= \zeta_A(y_A, z_A, y_B, z_B) \\ &= y_A - \frac{y_A^3}{3} - a - z_A + I, \end{aligned} \tag{4a}$$

$$\begin{aligned} \frac{dz_A}{dt} &= \epsilon\ \xi_A(y_A, z_A, y_B, z_B) \\ &= \epsilon\ (y_A - bz_A), \end{aligned} \tag{4b}$$

$$\begin{aligned} \frac{dy_B}{dt} &= \zeta_B(y_A, z_A, y_B, z_B) \\ &= y_B - \frac{y_B^3}{3} - a - z_B + \gamma(y_A - y_B), \end{aligned} \tag{4c}$$

$$\begin{aligned} \frac{dz_B}{dt} &= \epsilon\ \xi_B(y_A, z_A, y_B, z_B) \\ &= \epsilon\ (y_B - bz_B). \end{aligned} \tag{4d}$$

Here, y_A (y_B) is the membrane potential of $A(B)$ and z_A (z_B) represents a slow gating variable in $A(B)$.

The bifurcation structure of directed and undirected two-FN systems has been studied extensively from a numerical perspective.[11]

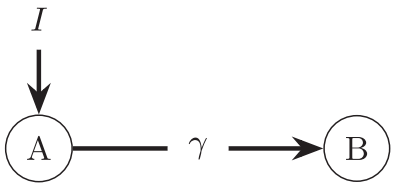

FIG. 2. A directed network of two FN model neurons, *A* and *B*. *A* receives an external input *I* and there is a unidirectional coupling from *A* to *B* with strength γ.

The bifurcation structure of the undirected system has been studied through analytical methods that leverage symmetry-based arguments or assume symmetric or near-symmetric FN models.[12,30,31] In contrast, we examine the system with asymmetry in both the external input and the coupling.

We begin by classifying the behavior of the two model neurons *A* and *B* in the I-γ parameter space, as shown in Fig. 3. Let I_{iA}, $I_{icA} \approx I_{isnA}$ for $i = 0, 1$ be the points associated to the FN model *A* for lower and upper Hopf bifurcations, canard explosions, and saddle node bifurcations, as defined in Sec. II. Regions (1)-(7) are described as follows:

(i) For $I < I_{0cA}$, both *A* and *B* will be quiescent at a stable equilibrium point. This corresponds to region (1) of Fig. 3. See Sec. V A for details.
(ii) For $I > I_{1cA}$, *A* becomes saturated and, as γ varies, there are three distinct behaviors for *B*. See Sec. V B for details. For $I > I_{1cA}$, there exist $I_{0cB}(I)$ and $I_{1B}(I)$ such that
  (a) For $\gamma < I_{0cB}(I)$, *B* is quiescent. This corresponds to region (2) in Fig. 3.
  (b) For $I_{0cB}(I) < \gamma < I_{1B}(I)$, *B* is firing. This corresponds to region (3) in Fig. 3.
  (c) For $\gamma > I_{1B}(I)$, *B* is saturated. This corresponds to region (4) in Fig. 3.
(iii) For $I_{0cA} < I < I_{1cA}$, *A* is firing and there are three distinct behaviors for *B*:
  (a) When $\gamma > 1 - b\epsilon$, *B* is phase locked with *A*, where the phases of the oscillating models remain separated by a constant offset, while amplitudes and waveforms may vary. This corresponds to region (5) of Fig. 3. See Sec. V C for details.
  (b) When $\gamma < 1 - b\epsilon$ and I is below a curve, denoted by $I_*(\gamma)$, MMOs or small canard oscillations may be present. This corresponds to region (6) of Fig. 3. See Sec. IV for the derivation and Sec. V D for details.
  (c) When $\gamma < 1 - b\epsilon$ and I is above $I_*(\gamma)$, *B* is firing and is phase locked with *A*. This corresponds to region (7) of Fig. 3. See Sec. IV for the derivation and Sec. V D for details.

In Sec. IV, we study the system (4) by applying geometric singular perturbation techniques. Leveraging fast-slow dynamics of (4), we reduce it to a two-dimensional singular limit. We analyze the resulting second-order dynamics and draw conclusions about canards and MMOs for the original dynamics (4) in Sec. V.

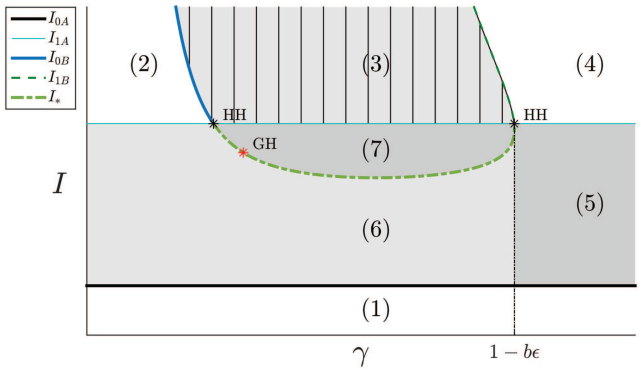

FIG. 3. Regions of behavior of the directed two-FN system (4) in the I-γ parameter space. Boundaries between regions are identified in the key. In regions (3), (5), (6), and (7), shaded gray, there is a stable limit cycle such that either *A* or *B* is firing. In region (3), with cross hatching, only *B* is firing. In regions (5) and (7), in darker gray, there is phase locking. In region (6), in light gray, *A* is firing and *B* may exhibit canard solutions. All boundaries are computed analytically. HH denotes a Hopf-Hopf bifurcation and GH denotes a generalized Hopf bifurcation.

IV. FAST-SLOW PHENOMENA IN THE DIRECTED TWO-FN SYSTEM

In this section, we assume *A* is firing and study the onset of firing in *B* as γ increases. This corresponds to region (6) of Fig. 3. We begin by providing definitions of canards and MMOs, which are observed numerically at the transition from quiescent to firing in *B* as shown in Fig. 4. For a general fast-slow system expressed as

$$\begin{aligned} \frac{d\mathbf{y}}{dt} &= \boldsymbol{f}(\mathbf{y}, \mathbf{z}), \\ \frac{d\mathbf{z}}{dt} &= \epsilon \boldsymbol{g}(\mathbf{y}, \mathbf{z}), \end{aligned} \tag{5}$$

$\mathbf{y} \in \mathbb{R}^m$ are fast variables, $\mathbf{z} \in \mathbb{R}^n$ are slow variables, and $0 < \epsilon \ll 1$ is the timescale separation parameter. The singular limit corresponding to $\epsilon = 0$ is called the *layer system*, $\frac{d\mathbf{y}}{dt} = \boldsymbol{f}(\mathbf{y}, \mathbf{z})$, where the slow variables $\mathbf{z}$ are parameters in this limiting system.

Definition IV.1 (Critical manifold). *Given system (5) with* $\epsilon = 0$, $C = \{(\mathbf{y}, \mathbf{z}) \in \mathbb{R}^m \times \mathbb{R}^n : \boldsymbol{f}(\mathbf{y}, \mathbf{z}) = \mathbf{0}\}$ *is called the critical manifold and corresponds to the equilibrium points of the layer system.*

Definition IV.2 (Normal hyperbolicity). *A subset* $C_h \subset C$ *is called normally hyperbolic if all the points of* C_h *are hyperbolic equilibrium points of the layer system, i.e., if* $D_{\mathbf{y}}\boldsymbol{f}$ *has no eigenvalues with zero real part.* C_h *is called attracting (respectively, repelling) if the eigenvalues have negative (respectively, positive) real part.* C_h *is a saddle if it is neither attracting nor repelling.*

Definition IV.3 (Fold points[55]). *Denote the set of points in C that are not normally hyperbolic (*$D_{\mathbf{y}}\boldsymbol{f}$ *has at least one eigenvalue with zero real part) as*

$$L := \left\{ (\mathbf{y}, \mathbf{z}) \in C \;\middle|\; \begin{array}{r} rank(D_{\mathbf{y}}\boldsymbol{f}[\mathbf{y}, \mathbf{z})] = m - 1 \\ \mathbf{l} \cdot D^2_{\mathbf{y}}\boldsymbol{f}(\mathbf{y}, \mathbf{z})(\mathbf{r}, \mathbf{r}) \neq 0 \\ \mathbf{l} \cdot D_{\mathbf{z}}\boldsymbol{f}(\mathbf{y}, \mathbf{z}) \neq \mathbf{0} \end{array} \right\},$$

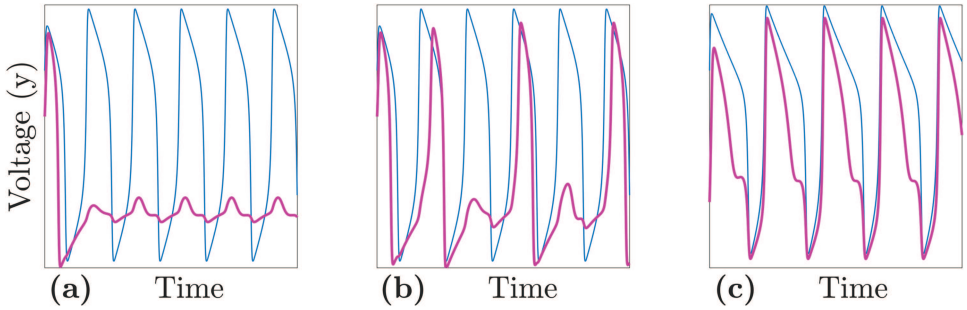

FIG. 4. Example of (a) canard solutions, (b) MMOs, and (c) phase locking.

where $\mathbf{l}$ *and* $\mathbf{r}$ *are corresponding left and right eigendirections of* $D_{\mathbf{y}}\boldsymbol{f}$. *L denotes the fold points of the critical manifold C. L locally divides the critical manifold C into subsets with different stability properties.*

Definition IV.4 (Canard). *A solution of (5) is called a canard if it stays within* $\mathcal{O}(\epsilon)$ *of a repelling branch of the critical manifold for a time that is* $\mathcal{O}(1)$ *on the slow timescale,* $\tau_1 = t\epsilon$.

Definition IV.5 [Mixed mode oscillation (MMO)[15]]. *Periodic solutions of (5) with peaks of substantially different amplitudes are called MMOs. Canard solutions often comprise the small oscillations present in MMOs.*

Definition IV.6 (Phase locking). *Two oscillating signals are said to be phase locked if the phases of the signals remain separated by a constant offset.*

An example of a canard solution, MMOs, and phase locking found in the directed two-FN system are shown in Fig. 4.

One of our goals is to show the existence of canards and MMOs in the two-FN system. In what follows, we review how the equilibrium points and the fold points of a fast-slow system play important roles in the existence of canards and MMOs. To this end, we study the behavior of the slow system on the critical manifold, which is called the reduced system. By the Fenichel theory, the equilibrium points of the full system lie within an $\mathcal{O}(\epsilon)$ neighborhood of the equilibrium points of the reduced system. However, the solutions of the reduced system blow up in finite time at the fold points. To remove these solutions, we study the desingularized system, which is obtained from the reduced system by an appropriate time rescaling. The equilibrium points of the desingularized system are within an $\mathcal{O}(\epsilon)$ neighborhood of the equilibrium points of the full system and the fold points.

In the slow timescale $\tau_1 = t\epsilon$, system (5) becomes

$$\begin{aligned} \epsilon \frac{d\mathbf{y}}{d\tau_1} &= \boldsymbol{f}(\mathbf{y},\mathbf{z}), \\ \frac{d\mathbf{z}}{d\tau_1} &= \boldsymbol{g}(\mathbf{y},\mathbf{z}). \end{aligned} \tag{6}$$

For this system, the singular limit corresponding to $\epsilon = 0$ is called the *reduced system* which is the differential algebraic equation corresponding to the slow dynamics $\frac{d\mathbf{z}}{d\tau_1} = \boldsymbol{g}(\mathbf{y},\mathbf{z})$ defined on the critical manifold C. Note that the full and reduced systems have the same equilibrium points.

To derive the desingularized system, we first differentiate $\boldsymbol{f}(\mathbf{y},\mathbf{z}) = 0$ with respect to τ_1 to get

$$(D_{\mathbf{y}}\boldsymbol{f}) \cdot \frac{d\mathbf{y}}{d\tau_1} + (D_{\mathbf{z}}\boldsymbol{f}) \cdot \frac{d\mathbf{z}}{d\tau_1} = \mathbf{0}. \tag{7}$$

Multiplying both sides of (7) by $\mathrm{adj}(D_{\mathbf{y}}\boldsymbol{f})$, the adjugate (or the transpose of the cofactor matrix) of $D_{\mathbf{y}}\boldsymbol{f}$, gives

$$-\det(D_{\mathbf{y}}\boldsymbol{f})\frac{d\mathbf{y}}{d\tau_1} = \mathrm{adj}(D_{\mathbf{y}}\boldsymbol{f})(D_{\mathbf{z}}\boldsymbol{f}) \cdot \boldsymbol{g}(\mathbf{y},\mathbf{z}). \tag{8}$$

This system is singular when $\det(D_{\mathbf{y}}\boldsymbol{f}) = 0$, namely, at fold points. This means that standard existence and uniqueness results do not hold at the fold points. However, rescaling time in (8) by $d\tau_1 = -\det(D_{\mathbf{y}}\boldsymbol{f})d\tau_2$ yields the desingularized system

$$\frac{d\mathbf{y}}{d\tau_2} = \mathrm{adj}(D_{\mathbf{y}}\boldsymbol{f})(D_{\mathbf{z}}\boldsymbol{f}) \cdot \boldsymbol{g}(\mathbf{y},\mathbf{z}). \tag{9}$$

Note that to obtain the corresponding flows of the reduced system from the desingularized system, due to the time scaling $d\tau_1 = -\det(D_{\mathbf{y}}\boldsymbol{f})d\tau_2$, the direction of the flows of the desingularized system must be reversed on branches where $\det(D_{\mathbf{y}}\boldsymbol{f}) > 0$.

The desingularized system (9) has two types of equilibrium points, which are called ordinary and folded singularities, respectively.

Definition IV.7 (Ordinary singularity). *An equilibrium point of the desingularized system is an ordinary singularity if it corresponds to an equilibrium point of the reduced system and lies within an* $\mathcal{O}(\epsilon)$ *neighborhood of an equilibrium point of the full system. Conditions for an ordinary singularity are*

$$\boldsymbol{g}(\mathbf{y},\mathbf{z}) = 0, \quad \det(D_{\mathbf{y}}\boldsymbol{f}) \neq 0, \quad \mathrm{adj}(D_{\mathbf{y}}\boldsymbol{f})(D_{\mathbf{z}}\boldsymbol{f}) \cdot \boldsymbol{g}(\mathbf{y},\mathbf{z}) \neq \mathbf{0}.$$

Definition IV.8 (Folded singularity). *An equilibrium point of the desingularized system is a folded singularity if it corresponds to a fold point of the reduced system. Conditions for a folded singularity are*

$$\det(D_{\mathbf{y}}\boldsymbol{f}) = 0, \quad \mathrm{adj}(D_{\mathbf{y}}\boldsymbol{f})(D_{\mathbf{z}}\boldsymbol{f}) \cdot \boldsymbol{g}(\mathbf{y},\mathbf{z}) = \mathbf{0}.$$

Suppose that the desingularized system (9) possesses a stable folded singularity $\mathbf{y}^*$ that is a node. Let the eigenvalues of the linearization of (9) at $\mathbf{y}^*$ be λ_s and λ_w, where $\lambda_s < \lambda_w < 0$. The trajectory tangent to the eigendirection corresponding to λ_s, called the *strong singular canard*, corresponds to a trajectory in the full system that

passes through a point close to $\mathbf{y}^*$ from the attracting branch to the repelling branch of the critical manifold. It creates a *funnel* such that all the trajectories in the full system that enter the funnel pass through the same point from the attracting branch to the repelling branch of the critical manifold. It was shown[16] that these trajectories rotate about the eigendirection corresponding to λ_w, called the *weak singular canard*, and eventually leave the funnel and jump away from the point near $\mathbf{y}^*$.[23] If there exists a *return mechanism* to return these trajectories back to the funnel, then MMOs occur.[21,22]

The remainder of this section details the calculations involved in the transformation of (4) into a two-dimensional desingularized system.

In Sec. V, we show conditions on I and γ such that the desingularized system possesses a stable folded node and thus a strong singular canard. We also explain the existence of a return mechanism and provide conditions for regions where MMOs are possible.

A. The critical manifold and fold points of the directed two-FN system

The critical manifold of system (4) with $\epsilon = 0$ is

$$C = \left\{ y_A, y_B, z_A, z_B \;\middle|\; \begin{array}{l} z_A = y_A - \frac{y_A^3}{3} - a + I \\ z_B = y_B - \frac{y_B^3}{3} - a + \gamma(y_A - y_B) \end{array} \right\}. \tag{10}$$

By Fenichel's theorem, the slow dynamics of the two-FN system (4) will lie $\mathcal{O}(\epsilon)$ away from C_h, the normally hyperbolic submanifold of C, on a normally hyperbolic slow invariant manifold C_ϵ with the same stability properties as C_h.[15,55]

We next identify fold points by checking the three conditions that determine the set L from Definition IV.3. The first eigenvalue of $D_{\mathbf{y}}\boldsymbol{\zeta}$ is $1 - y_A^2$, with left and right eigenvectors $\mathbf{l}_1 = \left[1, (\gamma - y_A^2 + y_B^2)/\gamma\right]$ and $\mathbf{r}_1 = (0,1)^\top$. The second eigenvalue of $D_{\mathbf{y}}\boldsymbol{\zeta}$ is $1 - y_B^2 - \gamma$, with left and right eigenvectors $\mathbf{l}_2 = (0,1)$ and $\mathbf{r}_2 = \left[1, (-\gamma + y_A^2 - y_B^2)/\gamma\right]^\top$.

The first condition is satisfied, i.e., $\mathrm{rank}(D_{\mathbf{y}}\boldsymbol{\zeta}) = 1$, if either $1 - y_A^2 = 0$ or $1 - y_B^2 - \gamma = 0$, but not both. The second condition is satisfied if

$$\mathbf{l} \cdot D_{\mathbf{y}}^2\boldsymbol{\zeta}\,(\mathbf{r},\mathbf{r}) = \mathbf{l} \cdot \begin{pmatrix} -2y_A & 0 & 0 & 0 \\ 0 & 0 & 0 & -2y_B \end{pmatrix} \begin{pmatrix} \mathbf{r} \\ \mathbf{r} \end{pmatrix} \neq 0.$$

For each eigenvalue, the condition becomes $y_B[(1 - y_A^2) - (1 - y_B^2 - \gamma)] \neq 0$, which is satisfied if the first condition is satisfied and $y_B \neq 0$. The third condition is always satisfied.

B. Desingularization of the directed two-FN system

According to (9), the desingularization of the reduced system of the two-FN system is

$$\frac{d\mathbf{y}}{d\tau_2} = \mathrm{adj}(D_{\mathbf{y}}\boldsymbol{\zeta})(D_{\mathbf{z}}\boldsymbol{\zeta}) \cdot (\mathbf{y} - b\mathbf{z}) \tag{11}$$

or equivalently,

$$\begin{aligned} \frac{dy_A}{d\tau_2} &= \rho_1(y_A, y_B) \\ &= -(1 - y_B^2 - \gamma)(y_A - bz_A), \\ \frac{dy_B}{d\tau_2} &= \rho_2(y_A, y_B) \\ &= \gamma(y_A - bz_A) - (1 - y_A^2)(y_B - bz_B), \end{aligned} \tag{12}$$

where z_A and z_B are defined as

$$\begin{aligned} z_A &= y_A - \frac{y_A^3}{3} - a + I, \\ z_B &= y_B - \frac{y_B^3}{3} - a + \gamma(y_A - y_B). \end{aligned} \tag{13}$$

In what follows, we study the stability type of the ordinary singularity and the folded singularities of (12). These points correspond to the equilibrium point and the fold points of the two-FN system, respectively. However, due to the time reversal step, the stability in the desingularized system is not identical to the stability of the full system.

By Definition IV.7, the ordinary singularity in (12) satisfies

$$\mathbf{y} - b\mathbf{z} = 0, \quad \det(D_{\mathbf{y}}\boldsymbol{\zeta}) \neq 0, \quad \mathrm{adj}(D_{\mathbf{y}}\boldsymbol{\zeta})(D_{\mathbf{z}}\boldsymbol{\zeta}) \cdot (\mathbf{y} - b\mathbf{z}) \neq \mathbf{0}.$$

Figure 5 depicts regions in I-γ parameter space according to the local stability of the ordinary singularity. Changes in stability in (12) correspond to Hopf bifurcations in (4). However, the curves in I-γ space that delineate the different signs of the real parts of the eigenvalues are slightly different from the Hopf bifurcation curves because predictions from singular perturbation analysis are accurate up to $\mathcal{O}(\epsilon)$. In regions where A and B are both quiescent or saturated (dark gray), the real parts of both eigenvalues are positive and the ordinary singularity is an unstable equilibrium. In regionswhere both A and B

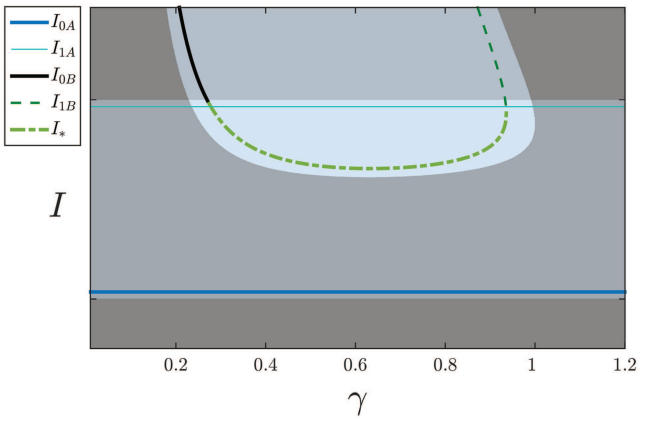

FIG. 5. Regions in the I-γ parameter space distinguishing local stability of the ordinary singularity in the desingularized system (12). Dark gray indicates an unstable node, light blue indicates a stable node, and light gray indicates a saddle. The Hopf bifurcations and distinguishing features of the original two-FN system (4), the boundaries in Fig. 3, are plotted for comparison as five curves.

are firing (light blue), the real parts of both eigenvalues are negative and the ordinary singularity is a stable equilibrium. In regions where either A or B is firing (light gray), the ordinary singularity is a saddle.

By Definition IV.8, the folded singularities of (12) satisfy

$$\det(D_{\mathbf{y}}\boldsymbol{\zeta}) = 0 \quad \text{and} \quad \operatorname{adj}(D_{\mathbf{y}}\boldsymbol{\zeta})(D_{\mathbf{z}}\boldsymbol{\zeta}) \cdot (\mathbf{y} - b\mathbf{z}) = \mathbf{0}$$

or equivalently

$$(1 - y_{B*}^2 - \gamma)(1 - y_{A*}^2) = 0, \tag{14a}$$

$$(1 - y_{B*}^2 - \gamma)(y_{A*} - bz_{A*}) = 0, \tag{14b}$$

$$(1 - y_{A*}^2)(y_{B*} - bz_{B*}) - \gamma(y_{A*} - bz_{A*}) = 0. \tag{14c}$$

Equation (14a) is satisfied when $y_{A*} = \pm 1$ or $y_{B*} = \pm\sqrt{1-\gamma}$. If (14b) and (14c) are satisfied but (14a) is not satisfied, the corresponding singularity is an ordinary singularity.

First, consider the case in which $y_{A*} = \pm 1$. By (14b)–(14c), either $z_{A*} = \frac{1}{b}y_{A*}$ or $\gamma = 0$ and $y_{B*} = \pm 1$. If $z_{A*} = \frac{1}{b}y_{A*}$ then, by (13), $I = \pm\frac{1}{b} \mp \frac{2}{3} + a$. Thus, we do not consider the case $y_{A*} = \pm 1$ further, since either $\gamma = 0$ or I is independent of γ.

When $y_{B*} = \pm\sqrt{1-\gamma}$, we use (13) to solve (14c) for y_{A*}, which is equivalent to solving the cubic equation

$$\beta_3 y_{A*}^3 + \beta_2 y_{A*}^2 + \beta_1 y_{A*} + \beta_0 = 0, \tag{15}$$

where

$$\beta_0 = b\gamma(I - a) + y_{B*} + b\left(-y_{B*} + \frac{y_{B*}^3}{3} + a + \gamma y_{B*}\right),$$

$$\beta_1 = -b\gamma,$$

$$\beta_2 = -y_{B*} + b\left(y_{B*} - \frac{y_{B*}^3}{3} - a - \gamma y_{B*}\right),$$

$$\beta_3 = \frac{2b\gamma}{3}.$$

The solutions of (15) for y_{A*} as a function of γ and I are given by

$$y_{A*,k} = -\frac{1}{3\beta_3}\left(\beta_2 + C_k + \frac{\beta_2^2 - 3\beta_1\beta_3}{C_k}\right),$$

where for $k = 1, 2, 3$,

$$C_k = \left(\frac{\sqrt{-3}-1}{2}\right)^{k-1}\left(\frac{\sigma - \sqrt{-27\beta_3^2\Delta}}{2}\right)^{1/3},$$

$$\Delta = 18\beta_3\beta_2\beta_1\beta_0 - 4\beta_0\beta_2^3 + \beta_2^2\beta_1^2 - 4\beta_3\beta_1^3 - 27\beta_3^2\beta_0^2,$$

$$\sigma = 2\beta_2^2 - 9\beta_3\beta_2\beta_1 + 27\beta_3^2\beta_0.$$

If $\Delta > 0$, there are three real solutions, i.e., three folded singularities, and if $\Delta < 0$, there is one real solution, i.e., one folded singularity.

The Jacobian of (12) for the folded singularities with $y_{B*} = \pm\sqrt{1-\gamma}$ has the form

$$D_{\mathbf{y}}\boldsymbol{\rho}(y_{A*}, y_{B*}) = \begin{pmatrix} 0 & 2y_{B*}\xi_A \\ \gamma + 2y_{A*}\xi_B & -(1 - y_{A*}^2) \end{pmatrix},$$

where $\boldsymbol{\rho} = (\rho_1, \rho_2)^\top$, $\xi_A = y_{A*} - bz_{A*}$, and $\xi_B = y_{B*} - bz_{B*}$. To classify each folded singularity, we use the trace and determinant of the Jacobian, which are

$$\operatorname{Tr}[D_{\mathbf{y}}\boldsymbol{\rho}(y_{A*}, y_{B*})] = -(1 - y_{A*}^2),$$

$$\det[D_{\mathbf{y}}\boldsymbol{\rho}(y_{A*}, y_{B*})] = 2y_{B*}\xi_A\left(\gamma + 2y_{A*}\xi_B\right).$$

When $\det(D_{\mathbf{y}}\boldsymbol{\rho}[y_{A*}, y_{B*}]) > 0$, the real parts of the eigenvalues have the same sign, so the singularity is a folded node or focus. The stability can be determined by looking at the sign of the trace. When $\det[D_{\mathbf{y}}\boldsymbol{\rho}(y_{A*}, y_{B*})] < 0$, the real parts of the eigenvalues have opposite signs, and the singularity is a folded saddle.

Figure 6 depicts regions in I-γ parameter space according to the local stability of the folded singularities. The white regions in this figure correspond to values of I and γ, where the given folded singularity does not exist in the desingularized system (12) (i.e., $\Delta < 0$).

V. DYNAMICS BY REGION

In this section, we apply the analytical results for the desingularized system (12) to draw conclusions about the original system (4). In doing so, we provide details of the computations used to produce Fig. 3 and the characterization of each of the seven regions, as described in Sec. III. We prove the stability of limit cycles of the Hopf bifurcations in model neuron B. We prove necessary conditions for MMOs and sufficient conditions for phase locking in terms of I and γ.

In the following proposition, we compute the value of the unique equilibrium point of (4), when Assumption II.1 holds, and its stability as a function of I and γ.

Proposition V.1. *Consider the directed two-FN system (4) and let Assumption II.1 hold. For any fixed I and γ, there exists a unique equilibrium point denoted by $\mathbf{p}_* = [y_{A*}(I), z_{A*}(I), y_{B*}(I,\gamma), z_{B*}(I,\gamma)]$. Then,*

1. *$\mathbf{p}_*$ is nonhyperbolic if I and γ satisfy*

$$\begin{aligned} &\sigma_1(I,\gamma) = 1 - b\epsilon - y_{A*}^2 = 0, \\ \text{or} \quad &\sigma_2(I,\gamma) = 1 - b\epsilon - \gamma - y_{B*}^2 = 0, \end{aligned} \tag{16}$$

   where σ_1 is the sum of the first two eigenvalues of the Jacobian of (4) evaluated at $\mathbf{p}_*$ and σ_2 is the sum of the second two eigenvalues of the Jacobian of (4) evaluated at $\mathbf{p}_*$.
2. *$\mathbf{p}_*$ is hyperbolic if I and γ do not satisfy (16). If $\sigma_1(I,\gamma) < 0$ and $\sigma_2(I,\gamma) < 0$, $\mathbf{p}_*$ is attracting. If $\sigma_1(I,\gamma) > 0$ and $\sigma_2(I,\gamma) > 0$, $\mathbf{p}_*$ is repelling. If $\sigma_1(I,\gamma)\sigma_2(I,\gamma) < 0$, $\mathbf{p}_*$ is a saddle.*

Proof. Solving for the equilibrium point of (4), we first compute y_{A*} as a function of I as

$$y_{A*} = \left(\frac{3(I-a)}{2} + \sqrt{\frac{[3(I-a)]^2}{4} + \tilde{b}^3}\right)^{1/3} + \left(\frac{3(I-a)}{2} - \sqrt{\frac{[3(I-a)]^2}{4} + \tilde{b}^3}\right)^{1/3}, \tag{17}$$

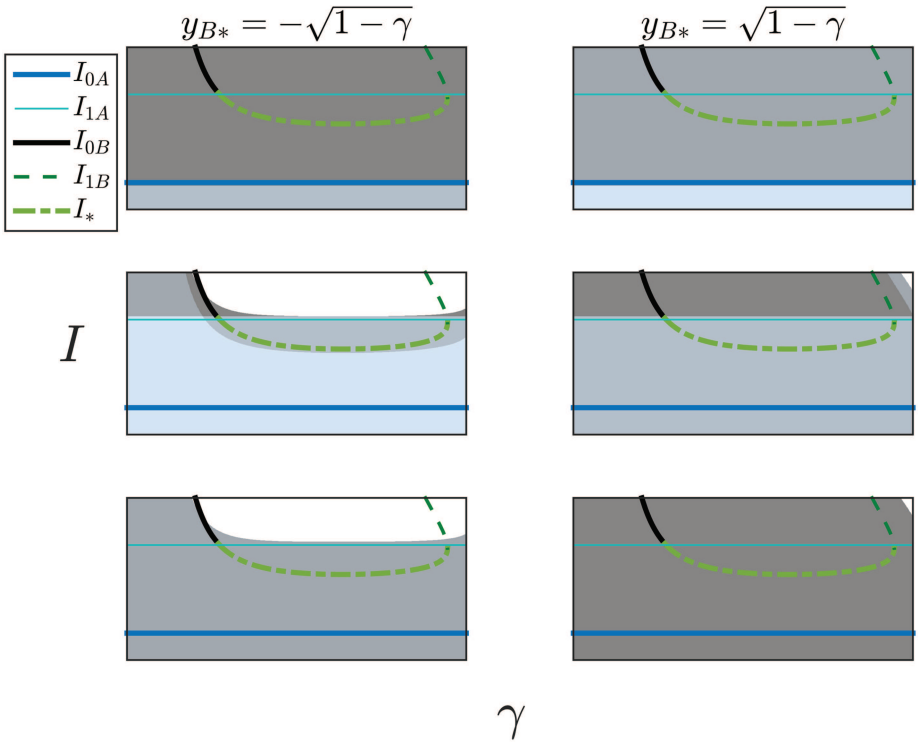

FIG. 6. Regions in the I-γ parameter space distinguishing local stability of the three folded singularities corresponding to $y_{B*} = -\sqrt{1-\gamma}$ (top, middle, and bottom plots on the left) and the three folded singularities corresponding to $y_{B*} = \sqrt{1-\gamma}$ (top, middle, and bottom plots on the right). In white regions, the folded singularity does not exist. In dark gray regions, the folded singularity is unstable. In light gray regions, the folded singularity is a saddle. In light blue regions, the folded singularity is stable.

where $\tilde{b} = \frac{1}{b} - 1$. Similarly, by leveraging (17), we can write y_{B*} as a function of I and γ as

$$y_{B*} = \left(\frac{3(\gamma y_{A*} - a)}{2} + \sqrt{\frac{9(\gamma y_{A*} - a)^2}{4} + \left(\tilde{b} + \gamma\right)^3}\right)^{1/3} + \left(\frac{3(\gamma y_{A*} - a)}{2} - \sqrt{\frac{9(\gamma y_{A*} - a)^2}{4} + \left(\tilde{b} + \gamma\right)^3}\right)^{1/3}. \quad (18)$$

Then, $z_{A*} = \frac{1}{b} y_{A*}$ and $z_{B*} = \frac{1}{b} y_{B*}$.

We compute the linearization of (4) around $\mathbf{p}_*$. We let $\boldsymbol{\nu}_A = (y_A, z_A)$, $\boldsymbol{\nu}_B = (y_B, z_B)$, and $\boldsymbol{\xi} = (\zeta_A, \epsilon\xi_A, \zeta_B, \epsilon\xi_B)$. The Jacobian of (4) evaluated at $\mathbf{p}_*$ is

$$D_{(\boldsymbol{\nu}_A, \boldsymbol{\nu}_B)}\boldsymbol{\xi}(\mathbf{p}_*) = \begin{pmatrix} 1 - y_{A*}^2 & -1 & 0 & 0 \\ \epsilon & -b\epsilon & 0 & 0 \\ \gamma & 0 & 1 - y_{B*}^2 - \gamma & -1 \\ 0 & 0 & \epsilon & -b\epsilon \end{pmatrix}.$$

The linearization is block triangular, so the eigenvalues of the Jacobian are the union of the eigenvalues of the diagonal blocks. This means that local stability can be determined through linearization of each FN model separately. The eigenvalues for the first and second blocks are

$$\lambda_{1,2} = \frac{1}{2}\left(1 - b\epsilon - y_{A*}^2\right) \pm \frac{1}{2}\sqrt{(1 - b\epsilon - y_{A*}^2)^2 - 4\epsilon(1 - b + y_{A*}^2 b)},$$

$$\lambda_{3,4} = \frac{1}{2}\left(1 - b\epsilon - \gamma - y_{B*}^2\right) \pm \frac{1}{2}\sqrt{(1 - b\epsilon - \gamma - y_{B*}^2)^2 - 4\epsilon(1 - b + y_{B*}^2 b + \gamma)}.$$

The sign of the real part of the eigenvalues will be determined by the sign of the first term. The first term of $\lambda_{1,2}$ is zero when $\sigma_1(I, \gamma) = \lambda_1 + \lambda_2 = 1 - b\epsilon - y_{A*}^2 = 0$. The first term of $\lambda_{3,4}$ is zero when $\sigma_2(I, \gamma) = \lambda_3 + \lambda_4 = 1 - b\epsilon - \gamma - y_{B*}^2 = 0$. Thus, $\mathbf{p}_*$ is non-hyperbolic when $\sigma_1 = 0$ or $\sigma_2 = 0$.

The stability of $\mathbf{p}_*$ when $\sigma_1\sigma_2 \neq 0$ is derived from the signs of the real parts of the eigenvalues of $D_{(\boldsymbol{\nu}_A, \boldsymbol{\nu}_B)}\boldsymbol{\xi}$. □

Remark V.2. *The one-dimensional manifolds of nonhyperbolic equilibrium points in I-γ space, $\{(I, \gamma) : \sigma_1(I, \gamma) = 0$ or $\sigma_2(I, \gamma) = 0\}$, correspond to the points where A and B undergo Hopf bifurcations.*

Remark V.3. *The corresponding flows of the full system and desingularized system have opposite sign when $\det(D_{\mathbf{y}}\boldsymbol{f}) > 0$ due to the time rescaling step, $d\tau_1 = -\det(D_{\mathbf{y}}\boldsymbol{f})d\tau_2$. One consequence is that when the ordinary singularity in the desingularized system is an unstable node, the unique equilibrium point in the full system is stable. Likewise, when the ordinary singularity in the desingularized system*

is a stable node, the unique equilibrium point in the full system is unstable.

A. Quiescence: Region (1)

Given the two-FN system (4) and Assumption II.1, if $I < I_{0cA}$, then A converges to a single stable equilibrium point, (y_{A*}, z_{A*}), which is quiescent. The value y_{A*}, independent of γ, is too low to induce firing in B, i.e., B is quiescent.

To fully understand the behavior of B, we examine the desingularized system (12), which has seven singularities for the parameter values in region (1). These include one unstable ordinary singularity (corresponding to the unique stable equilibrium point), one unstable folded node, two stable folded singularities, and three saddle folded singularities.

Due to the presence of a stable folded node when γ is close to 1 and $I < I_0$, robust families of canards that compose small oscillations of B could arise for these parameter values in the original system (4) in region (1) as described in Sec. IV.

B. Hopf bifurcations in B: Regions (2), (3), and (4)

For the two-FN system (4), if $I > I_{1cA}$ then A is saturated. We prove conditions for when B will be quiescent, firing, or saturated and provide illustrative examples of the desingularized system nullclines and phase plane for representative parameter values.

Proposition V.4. *Consider the two-FN system (4) and Assumption II.1. Let $I > I_{1cA}$ and $\gamma < 1 - b\epsilon$. There exist two curves of Hopf bifurcations defined by*

$$I_{1B,0B}(\gamma) = \tilde{b} y_{A*\pm} + \frac{y_{A*\pm}^3}{3} + a,$$

where

$$y_{A*\pm} = \pm\frac{1}{\gamma}\left(\frac{1}{3}(1-\epsilon b-\gamma)^{3/2} + \left(\tilde{b}+\gamma\right)\sqrt{1-\epsilon b-\gamma} + a\right).$$

The bifurcation structure of B in the small parameter range around the transition from quiescent to firing is analogous to the single FN model in Sec. II. There is a saddle node bifurcation of limit cycles at $I = I_{0sn}(\gamma)$, canard explosion at $I = I_{0cB}(\gamma)$, and Hopf bifurcation at $I = I_{0B}(\gamma)$. B transitions from firing to saturated through a supercritical Hopf bifurcation at $I = I_{1B}(\gamma)$.

Moreover, there exists γ_* such that, for $I < I_{0B}(\gamma_*)$, the following holds. If $\gamma < \gamma*$, the Hopf bifurcation at $I_{0B}(\gamma)$ is subcritical and, if $\gamma > \gamma*$, the Hopf bifurcation at $I_{0B}(\gamma)$ is supercritical.

Proof. The Hopf bifurcations in B occur at nonhyperbolic equilibrium points, which are $y_{B*\pm} = \pm\sqrt{1-\gamma-b\epsilon}$ by Proposition V.1.

Substituting $y_{B*\pm} = \pm\sqrt{1-\gamma-b\epsilon}$ and (4d) into the equilibrium solution for (4c) gives the critical values

$$y_{A*\pm} = \pm\frac{1}{\gamma}\left(\frac{1}{3}(1-\epsilon b-\gamma)^{3/2} + \left(\tilde{b}+\gamma\right)\sqrt{1-\epsilon b-\gamma} + a\right).$$

Substituting $y_{A*\pm}$ and (4b) into (4a) gives the values

$$I_{1B,0B} = \tilde{b} y_{A*\pm} + \frac{y_{A*\pm}^3}{3} + a.$$

For a fixed γ, we check the conditions of Proposition .4 for the bifurcation parameter I. First, we transform (y_{B*}, z_{B*}) to the origin $(0,0)$, by introducing $y_0 = y_B - y_{B*}$ and $z_0 = z_B - z_{B*}$. With this change of variables, the dynamics of B (4c)-(4d) can be expressed as

$$\begin{aligned}\frac{dy_0}{dt} &= (1-\gamma-y_{B*}^2)y_0 - \frac{y_0^3}{3} - y_0^2 y_{B*} - z_0,\\ \frac{dz_0}{dt} &= \epsilon(y_0 - bz_0)\end{aligned} \tag{19}$$

and the Jacobian of (19) evaluated at the origin is

$$J_B(0,0) = \begin{pmatrix} 1-y_{B*}^2-\gamma & -1 \\ \epsilon & -b\epsilon \end{pmatrix}.$$

Now we apply Proposition II.4.

Condition 1 of Proposition II.4: This condition holds because $\mathrm{Tr}[J_B(0,0)] = 0$ at the bifurcation values $I = I_{0B}$ and $I = I_{1B}$.

Condition 2 of Proposition II.4: The second condition holds as well because

$$\frac{\partial}{\partial I}\Re[\lambda_{3,4}(I)]\Big|_{I=I_{0B,1B}} \neq 0,$$

where $\lambda_{3,4}$ are given in the proof of Proposition V.1.

Condition 3 of Proposition 2.4: The cubic coefficient α of the Taylor expansion of (4c)–(4d) (Definition II.3) which determines whether the Hopf bifurcation is subcritical or supercritical,[46] is

$$\alpha = \frac{1}{8}\left(\frac{2b - 2b\gamma - b^2\epsilon - 1}{1-b^2\epsilon}\right).$$

At $\gamma = \gamma_*$, $\alpha = 0$ and B undergoes a "generalized Hopf," or Bautin, bifurcation, depicted in Fig. 3 as the point GH.[56,57] For $\gamma > \gamma_*, \alpha < 0$ and the limit cycles resulting from the Hopf bifurcations are stable (supercritical). Otherwise, the limit cycles are unstable and the bifurcations are subcritical, as for A. □

Remark V.5. *For the two-FN system (4), given Assumption II.1, if A is saturated, then B transitions from quiescent to firing to saturated as a function of I and γ.*

In region (2), the desingularized system (12) has seven singularities, one ordinary singularity and six folded singularities. The ordinary singularity is unstable, and there are three unstable folded singularities and three folded saddles. This is a region where A is saturated and B is quiescent, so the full two-FN system has a unique stable equilibrium point.

In region (3), the desingularized system (12) has seven singularities for small γ, and five singularities for large γ.

The transition from seven to five singularities occurs through a saddle node bifurcation between a folded saddle point and an unstable folded singularity. The ordinary singularity is a saddle and the unique equilibrium point of the full system is also a saddle.

In region (4), the desingularized system (12) can have one, three, five, or seven singularities. Parameter choices for (12) in which $\gamma > 1$, which corresponds to $\gamma > 1 - b\epsilon$ in the two-FN system, result in one singularity. Since $\gamma > 1$ for (12) in region (4), the folded singularities corresponding to $y_{B*} = \pm\sqrt{1-\gamma}$ no longer exist. The ordinary singularity is unstable and the unique equilibrium point of the full system is stable.

C. Phase-locking: Region (5)

Consider the two-FN system (4) with $I_{0cA} < I < I_{1cA}$ such that A is firing. Region (5) corresponds to this range of I and $\gamma > 1 - b\epsilon$. For $I_{0A} < I < I_{1A}$ and $\gamma > 1 - b\epsilon$, the linearization of (4) around the equilibrium point $\mathbf{p}_*$ has two eigenvalues $\lambda_{1,2}$ with positive real part, and two eigenvalues $\lambda_{3,4}$ with negative real part. Thus, B will follow the limit cycle from A.

Remark V.6. *For the two-FN system (4), given Assumption II.1, if A is firing and $\gamma > 1 - b\epsilon$, B is firing and A and B are phased locked.*

For the desingularized system (12), $\gamma > 1$ and the singularities at $y_{B*} = \pm\sqrt{1-\gamma}$ no longer exist. The ordinary singularity is a saddle and the unique equilibrium point of the full system is also a saddle. Note that there are still folded singularities corresponding to $y_{A*} = \pm 1$, but they are the points, I_{0A} and I_{1A}, where the stability changes in the ordinary singularity.

D. Mixed mode oscillations: Regions (6) and (7)

Now consider the two-FN system (4) when $I_{0cA} < I < I_{1cA}$ and $\gamma < 1 - b\epsilon$. In this case, a range of dynamics is observed in simulation. For $\gamma \ll 1$, the influence of A is small, so B exhibits only small oscillations that stay close to (y_{B*}, z_{B*}). As γ is increased, the influence of oscillation A can be large enough to yield a mixed mode oscillation (MMO), see Fig. 4(b). As γ is increased further and the influence of A becomes increasingly strong, B approaches firing at the same frequency as A.

To better understand these transitions, we study the bifurcation diagrams and phase planes of the desingularized system (12). We prove necessary conditions for the existence of MMOs as a function of I and γ.

In region (6), there are seven singularities for the desingularized system (12), seen in Figs. 7(a) and 7(b). In this region, the ordinary singularity of the desingularized system (12) is a saddle (corresponding to a saddle in the full system), whereas the folded singularities include three saddles, one stable folded singularity and two unstable singularities. Trajectories, nullclines, and singularities are shown in Fig. 7(a) for parameters in region (6). Co-existence of the stable folded node and a global return mechanism due to the S-shaped critical manifold allows the existence of canard-induced MMOs in this region of parameter space for the two-FN system.[21]

Figure 7(b) zooms in on the area around the ordinary singularity and stable folded node for the same parameter values as Fig. 7(a). Critical features for canard existence are present in this region. An unstable manifold of the ordinary singularity, which is a saddle, connects to the stable folded node, shown in red. The strong singular canard of the stable folded node is shown in green, and the stable manifold of the ordinary saddle singularity is shown in blue. All trajectories between the stable manifold of the ordinary singularity and the stable manifolds of the two folded saddles to the right of the stable folded node will be funneled to the stable folded node, and thus will pass from the attracting to repelling parts of the critical manifold in the full system. This results in the family of canard solutions seen in the full system.

In region (7), there are seven singularities. In this region, the ordinary singularity of the desingularized system (12) is stable (corresponding to an unstable equilibrium in the full system), whereas the folded singularities include four saddles and two unstable singularities. As a consequence, canard-induced MMOs do not exist in the two-FN system, and both A and B are firing and phase-locked.

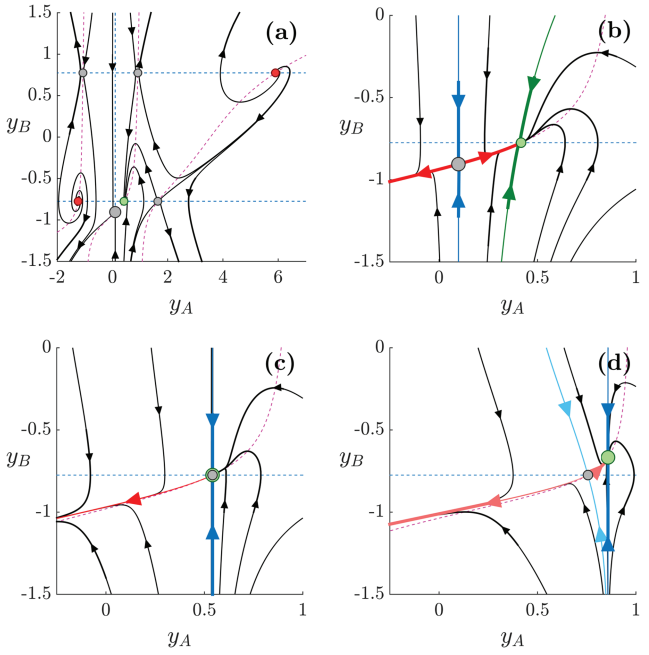

FIG. 7. Nullclines and phase planes for the desingularized system (12) near the boundary between regions (6) and (7). For all panels, the folded singularities are shown as smaller circles and the ordinary singularity is a larger circle. Green represents a stable singularity, gray represents a saddle, and red represents an unstable singularity. Trajectories of the system are shown in black. The y_A (blue dashed) and y_B (pink dashed) nullclines are also shown. Panels (a) and (b) show the phase plane for $I = 0.9$ and $\gamma = 0.4$ [in region (6)] for differing ranges of y_A and y_B. Panel (b) shows the stable (blue) and unstable (red) manifolds of the ordinary singularity, which is a saddle, along with the strong canard (green) associated with the stable folded node. Panel (c) shows the phase plane for $I = 1.0633$ and $\gamma = 0.4$ on the boundary between regions (6) and (7). Panel (d) shows the phase plane for $I = 1.3$ and $\gamma = 0.4$ in region (7), where A is firing and B is phase locked with A in the two-FN system (4). The stable (light blue) and unstable (light red) manifolds of the folded saddle are shown.

We next compute the boundary between regions (6) and (7), shown by I_* in Fig. 3. The boundary is defined by points at which there is a transcritical bifurcation between the ordinary singularity and a folded singularity, called FSN type II bifurcation, where the ordinary singularity transitions from a saddle to a stable node and the folded singularity transitions from a stable node to a saddle. This transcritical bifurcation is a known location for the onset of MMOs,[32] so computing I_* gives necessary conditions for the existence of MMOs. Figure 7(c) depicts the phase plane near the ordinary singularity at the transcritical bifurcation. The strong stable canard trajectory and connecting unstable manifold of the ordinary singularity are no longer present. Figure 7(d) depicts the phase plane near the ordinary singularity as I is increased beyond the transcritical bifurcation. In this region, there is no longer a stable folded node.

Proposition V.7 [Theorem 3.4.1 (modified)[46]]. *A system* $\dot{\boldsymbol{x}} = \boldsymbol{f}(\mathbf{x}, \mu)$, *admits a transcritical bifurcation at* $(\mathbf{x}_0, \mu_0)$ *if*

1. $D_{\mathbf{x}}\boldsymbol{f}(\mathbf{x}_0, \mu_0)$ *has a simple* 0 *eigenvalue with right eigenvector* $\boldsymbol{v}$ *and left eigenvector* $\boldsymbol{w}$.
2. $\boldsymbol{w}D^2_{\mathbf{x}\mu}\boldsymbol{f}(\mathbf{x}_0, \mu_0)\boldsymbol{v} \neq 0$.
3. $\boldsymbol{w}D^2_{\mathbf{x}}\boldsymbol{f}(\mathbf{x}_0, \mu_0)(\boldsymbol{v}^\top, \boldsymbol{v}^\top)^\top \neq 0$.

Proposition V.8. *Consider the desingularized system* (12) *with fixed* $\gamma < 1$ *and let*

$$I_*(\gamma) = \frac{1}{3b^3\gamma^3}\left(\sqrt{1-\gamma} + \frac{2b\sqrt[3]{1-\gamma}}{3} - ba\right)^3 + a. \tag{20}$$

Then, system (12) *admits a transcritical bifurcation at* $[\boldsymbol{p}, I_*(\gamma)]$, *where* $\boldsymbol{p} = (y_{A*}, y_{B*})^\top$ *is an ordinary singularity of* (12), *i.e.,* $\boldsymbol{p}$ *solves* (14b) *and* (14c).

Proof. To show the transcritical bifurcation, we apply Proposition V.7 to (12). The Jacobian, $D_{\mathbf{y}}\boldsymbol{\rho}$, of (12) is

$$\begin{pmatrix} -(1-y_B^2-\gamma)(1-b+by_A^2) & 2y_B(y_A - bz_A) \\ \gamma + 2y_A(y_B - bz_B) & -(1-y_A^2)(1-b+by_B^2+b\gamma) \end{pmatrix}.$$

Condition 1 of Proposition 5.7: Evaluating the Jacobian of (12) at $(y_A, y_B)^\top = \boldsymbol{p}$ and $I = I_*$ gives

$$D_{\mathbf{y}}\boldsymbol{\rho}(\boldsymbol{p}, I_*) = \begin{pmatrix} 0 & 0 \\ \gamma & -(1-y_{A*}^2) \end{pmatrix},$$

which has a zero eigenvalue with a left eigenvector $\boldsymbol{w} = (1, 0)$ and a right eigenvector $\boldsymbol{v} = \left(1, \frac{\gamma}{-(1-y_{A*}^2)}\right)^\top$.

Condition 2 of Proposition V.7: Taking the derivative of $D_{\mathbf{y}}\rho$ with respect to I and evaluating at $(y_A, y_B)^\top = \boldsymbol{p}$ and $I = I_*$ gives

$$D^2_{\mathbf{y}I}\boldsymbol{\rho}(\boldsymbol{p}, I_*) = \begin{pmatrix} 0 & -2by_{B*} \\ 0 & 0 \end{pmatrix}.$$

Then, multiplying $D^2_{\mathbf{y}}\boldsymbol{\gamma}\boldsymbol{\rho}(\boldsymbol{p}, I_*)$ from left by $\boldsymbol{w}$ and from right by $\boldsymbol{v}$, we have

$$\boldsymbol{w}\left[D^2_{\mathbf{y}}\boldsymbol{\gamma}\boldsymbol{\rho}(\boldsymbol{p}, I_*)\right]\boldsymbol{v} = \frac{2b\gamma y_{B*}}{1-y_{A*}^2},$$

which is always nonzero.

Condition 3 of Proposition V.7: Evaluating $D^2_{\mathbf{y}}\boldsymbol{\rho}$ at $\boldsymbol{p} = (y_A, y_B)^\top$ and $I = I_*$ gives

$$D^2_{\mathbf{y}}\boldsymbol{\rho}(\boldsymbol{p}, I_*) = \begin{pmatrix} 0 & 2y_{B*}(1-s) & 0 & 2y_{A*} \\ 2y_{B*}(1-s) & 0 & 2y_{A*} & -2y_{B*}s \end{pmatrix},$$

where $s = b(1-y_{A*}^2)$. Then, multiplying $D^2_{\mathbf{y}}\boldsymbol{\rho}$ from left by $\boldsymbol{w}$ and from right by $(\boldsymbol{v}^\top, \boldsymbol{v}^\top)^\top$, we have

$$\boldsymbol{w}\left[D^2_{\mathbf{y}}\boldsymbol{\rho}(\boldsymbol{p}, I_*)\right]\begin{pmatrix} \boldsymbol{v} \\ \boldsymbol{v} \end{pmatrix} = \frac{-2\gamma}{1-y_{A*}^2}\left\{y_{B*}[1-b(1-y_{A*}^2)] + y_{A*}\right\}, \tag{21}$$

which is also nonzero as shown in Fig. 8. □

A necessary condition for canard-induced MMOs is the existence of a stable folded node with a return mechanism, since the family of canard solutions that form the small oscillations are only found in this context.[32,58] The stable folded node has a corresponding family of canard solutions because there are many trajectories that cross from the attracting to the repelling branch of the critical manifold through the stable folded node. Furthermore, the return mechanism is required for MMOs because, after each relaxation oscillation or canard trajectory, the dynamics must return near the singularity in order for the MMO to persist.

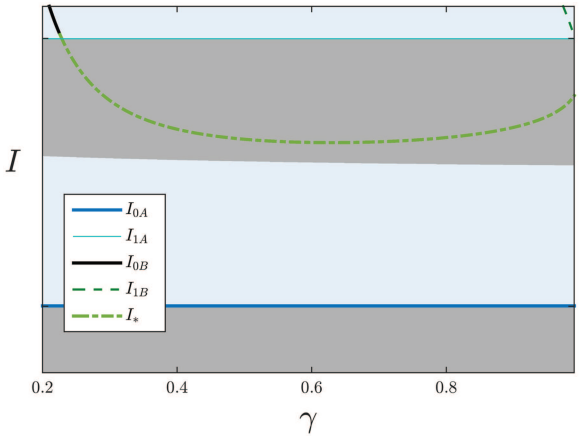

FIG. 8. Regions in the I-γ parameter space distinguishing the sign of (21). In the light blue regions, the sign is positive. In the light gray regions, the sign is negative. At the boundaries, the sign becomes zero. For all (I, γ) pairs on I_* (shown by the green dashed line), the sign of (21) is nonzero, except where I_* intersects I_{1A}. The bifurcation at the intersection is a codimension-two bifurcation.

Global return mechanism: For all coupling strengths $\gamma < 1 - b\epsilon$, the projection of the critical manifold in one fast and two slow dimensions is S-shaped, with two attracting branches connected by a repelling branch in the center and twofold lines. The relaxation oscillations in this setting provide a global return mechanism for the system.[21,32]

Stable folded node: In the directed two-FN system, MMOs are only possible for $I < I_*(\gamma)$, since that is where there is a stable folded node.

Remark V.9. *Consider the two-FN system* (4). *For* $I_{0cA} < I < I_*(\gamma)$, *this system exhibits MMOs and if* $I_*(\gamma) < I < I_{1cA}$, *it exhibits phase locking.*

Remark V.10. *A special case of the transcritical (FSN II) bifurcations occurs when* γ *and* I *satisfy* $I_*(\gamma) = I_{1A}$. *In this case, there is a codimension-two bifurcation where the real parts of the eigenvalues of the linearization of* (12) *about the ordinary singularity and the eigenvalues of the linearization of* (12) *about the folded singularity,* $y_{B*} = -\sqrt{1-\gamma}$, *are equal to zero. The codimension-two bifurcation is illustrated by the orange star in the bifurcation diagram of* (12) *in Fig. 9(a), for* $\gamma = 0.22$. *If we fix* $I_{0cA} < I < I_{1cA}$ *and decrease the value of* γ *below the codimension-two value, then MMOs are always possible.*

To highlight the location of the transcritical bifurcation (FSN II) and compare to features in Fig. 3, we show it as the blue star in the bifurcation diagram of (12) in Fig. 9(b). Here, by treating I as the bifurcation parameter, and maintaining γ fixed at value 0.4,

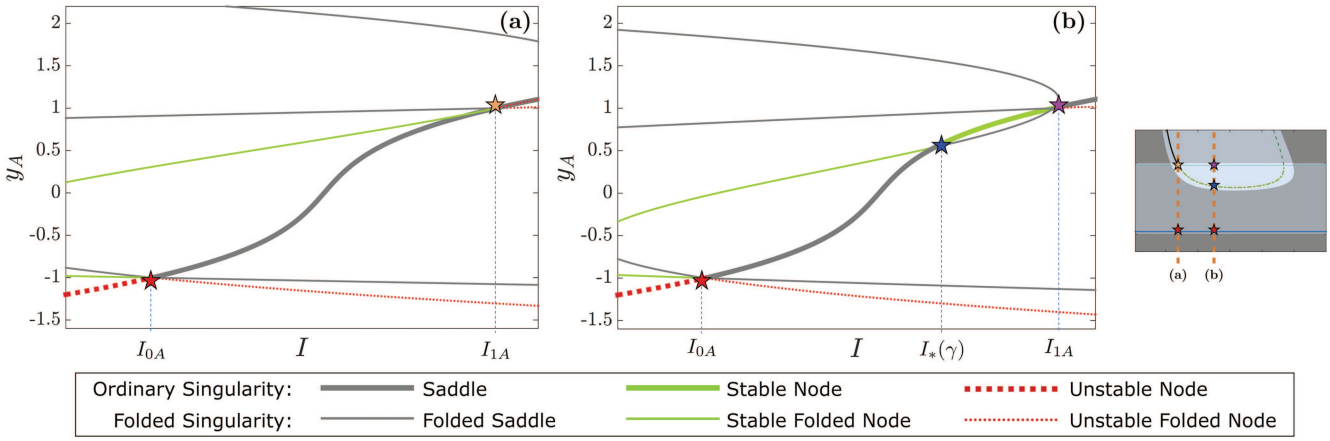

FIG. 9. Bifurcation diagrams of the desingularized system (12) with bifurcation parameter I for two different values of γ. The inset shows the locations of the two diagrams (dashed lines correspond to the I-axis) in I-γ parameter space matching Fig. 5. (a) When $\gamma = 0.22$, the desingularized system admits a codimension-two bifurcation (orange star), where the ordinary singularity remains a saddle, while one folded singularity switches from a stable folded singularity to an unstable folded singularity and the other switches from a folded saddle to an unstable folded singularity. (b) When $\gamma = 0.4$, a transcritical bifurcation (FSN II) occurs between the ordinary singularity and a folded singularity (blue star). For this choice of γ, the desingularized system admits another folded singularity (unstable folded singularity) at $y_{A*} \approx 6$, which is not shown in either figure.

we can observe that the ordinary singularity transitions from unstable (thick dashed red) to saddle (thick gray) at $I = I_{0A}$ (red star). Simultaneously, a stable folded singularity (thin green) becomes a folded saddle (thin gray) and a folded saddle becomes an unstable folded singularity (thin dashed red). The concurrent existence of a stable folded node and a folded saddle allows for *composite canards*, which are trajectories that follow canard solutions of at least two different folded singularities and produce complex small-amplitude oscillations.[59]

At $I = I_*(\gamma)$ (blue star), derived in Proposition V.8, the ordinary singularity and a folded singularity swap stability properties in a transcritical bifurcation, which can be classified as an FSN II bifurcation. Also, this FSN II bifurcation in the desingularized system (12) corresponds to the generalized Hopf bifurcation in the two-FN system (4). For $I > I_*$, (4) exhibits phase locking and MMOs are no longer possible.

At $I = I_{1A}$ (magenta star), the ordinary singularity returns to a saddle and two folded saddles become two unstable folded singularities. For $I > I_{1A}$, phase locking in (4) is no longer possible. We also note that when I is just above I_{1A}, one folded saddle merges with an unstable folded singularity through a saddle node bifurcation.

VI. DIRECTED TREE OF FN MODEL NEURONS

In this section, we consider an extension of the previous results to a directed chain of coupled FN models. We leverage the connection between the desingularized system and the directed two-FN system to find sufficient conditions for phase locking.

Consider a system of k FN model neurons with dynamics

$$\dot{\mathbf{x}} = \mathbf{f}(\mathbf{x}, \mathbf{I}, \boldsymbol{\gamma}),$$

where $\mathbf{x} \in \mathbb{R}^{2k}$, $\mathbf{I} \in \mathbb{R}^{k-1}$, and $\boldsymbol{\gamma} \in \mathbb{R}^{k-1}$. All FN models receive an external input except for the last in the chain. Then, by allowing heterogeneity in the external inputs and coupling strengths, the linearization around the equilibrium point can be expressed as

$$D_{\mathbf{x}}\mathbf{f} = \begin{pmatrix} J_1 & 0_{2\times2} & 0_{2\times2} & 0_{2\times2} & \cdots & 0_{2\times2} \\ \Gamma_1 & J_2 & 0_{2\times2} & 0_{2\times2} & \cdots & 0_{2\times2} \\ 0_{2\times2} & \Gamma_2 & J_3 & 0_{2\times2} & \ddots & \vdots \\ \vdots & \ddots & \ddots & \ddots & \ddots & 0_{2\times2} \\ 0_{2\times2} & 0_{2\times2} & \ddots & \Gamma_{k-2} & J_{k-1} & 0_{2\times2} \\ 0_{2\times2} & 0_{2\times2} & \cdots & 0_{2\times2} & \Gamma_{k-1} & J_k \end{pmatrix},$$

where the first diagonal block is given by

$$J_1 = \begin{pmatrix} 1 - y_1^2 & -1 \\ \epsilon & -b\epsilon \end{pmatrix}$$

and the subsequent diagonal blocks are given by

$$J_i = \begin{pmatrix} 1 - y_i^2 - \gamma_{i-1} & -1 \\ \epsilon & -b\epsilon \end{pmatrix}, \quad i \in \{2, \ldots, k\}.$$

The blocks on the lower diagonal are

$$\Gamma_i = \gamma_i \begin{pmatrix} 0 & 1 \\ 0 & 0 \end{pmatrix}, \quad i \in \{1, \ldots, k-1\}.$$

Due to the lower block triangular structure of the linearization, local stability of the equilibrium can be determined by studying the eigenvalues of the diagonal blocks. Similar to the analysis at the beginning of Sec. V, we begin by solving for the equilibrium point.

The equilibrium of the first model neuron is given by

$$y_{1*} = \left(\frac{3(I_1 - a)}{2} + \sqrt{\frac{[3(I_1 - a)]^2}{4} + \tilde{b}^3}\right)^{1/3} + \left(\frac{3(I_1 - a)}{2} - \sqrt{\frac{[3(I_1 - a)]^2}{4} + \tilde{b}^3}\right)^{1/3}.$$

The equilibrium of the i-th model neuron is given by

$$y_{i*} = \left(\frac{3\tilde{I}}{2} + \sqrt{\frac{(3\tilde{I})^2}{4} + \left(\tilde{b} + \gamma_{i-1}\right)^3}\right)^{1/3} + \left(\frac{3\tilde{I}}{2} - \sqrt{\frac{(3\tilde{I})^2}{4} + \left(\tilde{b} + \gamma_{i-1}\right)^3}\right)^{1/3},$$

where $\tilde{I} = \gamma_{i-1} y_{i-1*} + I_i - a$, $i \in \{2, \ldots, k\}$. The eigenvalues of the individual diagonal blocks are

$$\lambda_{1,2} = \frac{1}{2}\left(1 - y_{1*}^2 - b\epsilon\right) \pm \frac{1}{2}\sqrt{(y_{1*}^2 + b\epsilon - 1)^2 - 4\epsilon(1 - b + y_{1*}^2 b)},$$

$$\lambda_{2i-1,2i} = \frac{1}{2}\left(1 - y_{i*}^2 - \gamma_{i-1} - b\epsilon\right) \pm \frac{1}{2}\sqrt{(y_{i*}^2 + \gamma_{i-1} + b\epsilon - 1)^2 - 4\epsilon(1 - b + y_{i*}^2 b + \gamma_{i-1})},$$

where $i = 2, \ldots, k$. The Hopf bifurcations in the i-th model neuron occur at

$$I_{H\pm} = \pm\frac{1}{3}(1 - \gamma_{i-1} - b\epsilon)^{3/2} \pm \sqrt{1 - \gamma_{i-1} - b\epsilon}\left(\tilde{b} + \gamma_{i-1}\right) - \tilde{I}. \quad (22)$$

As a directed tree can be decomposed into a collection of directed chains, these results generalize to directed trees as well. In Fig. 10, we illustrate with the directed chain that starts with the light orange FN model and is directed to the right to the cyan FN model. The first FN model (light orange) receives an input $I = 1.2$, which ensures that it is firing. The coupling strength to the second FN model (dark orange) with input $I = 0.4$ ensures that the second FN model is in region (6) where MMOs are possible. However, in this case, no MMOs are exhibited. The coupling strength to the third FN model (dark cyan) with a zero input ensures that it is also in region (6). In this case, MMOs induced by canards are exhibited. The active signal has frequency half that of the first and second FN models. As a result, the input to the fourth FN model (cyan) is an MMO; this case was not covered in our two-FN system analysis. The fourth FN model responds to incoming canards with almost no activity and incoming spikes with a small canard. The frequency of the small canards in the fourth FN model is the same as the frequency of the active signal of the third FN model.

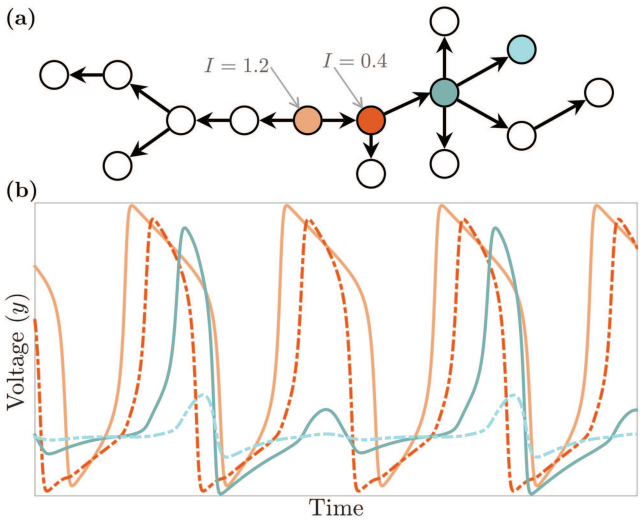

FIG. 10. Panel (a) depicts a directed tree graph of FN model neurons with heterogeneous external inputs I_i. All edge weights have coupling strength $\gamma = 0.07$. A representative chain is selected and indicated by vertices with colors matching simulation results, which are shown in panel (b). The frequency of the cyan FN models is half of the frequency of the orange FN models.

VII. DISCUSSION

In this work, we study a system of two FN model neurons in a setting where the first FN model has a constant external input I, the second FN model has no input, and there is a unidirectional coupling with strength γ from the first FN model to the second. We study and rigorously characterize all of the different regions of dynamic behavior for the two-FN system in I-γ space. We prove new necessary conditions in terms of both I and γ for the existence of canards and MMOs. We leverage this result to find a similarly new sufficient condition for phase locking and extend to systems of FN models in directed tree networks. We illustrate for a directed chain of four FN models, where canards, MMOs, and frequency halving is observed as predicted.

Further investigation of the two-FN system is needed to determine the threshold between MMOs and canard solutions without MMOs, which have been observed in simulation. This threshold has been studied numerically, as well as the chaotic behavior at the boundaries between types of MMOs, e.g., in Ref. 11. An analytical understanding of the threshold phenomena involved in the onset of firing in systems of FN models would add significantly to the literature on canards and MMOs.

Future directions include consideration of more diverse graph structures that include loops within the graph and a more detailed analysis of the MMOs in these systems. General results have been found for finite dimensional fast-slow systems, which could be applied in this context.[20] Incorporating heterogeneous model parameters is another area of future investigation. Changing ϵ changes the frequency of oscillation and the timescale of the FN model, so a network of FN models with differing values of ϵ would be a compelling

system for exploring canard phenomena in three or more distinct timescales.

ACKNOWLEDGMENTS

This work was jointly supported by the National Science Foundation under NSF-CRCNS Grant No. DMS-1430077 and the Office of Naval Research under ONR Grant No. N00014-14-1-0635. This material is also based upon work supported by the National Science Foundation Graduate Research Fellowship under Grant No. DGE-1656466. Any opinion, findings, and conclusions or recommendations expressed in this material are those of the authors and do not necessarily reflect the views of the National Science Foundation.

REFERENCES

[1] A. L. Hodgkin and A. F. Huxley, "A quantitative description of membrane current and its application to conduction and excitation in nerve," J. Physiol. **117**, 500–544 (1952).
[2] R. FitzHugh, "Mathematical models of threshold phenomena in the nerve membrane," Bull. Math. Biophys. **17**, 257–278 (1955).
[3] R. FitzHugh, "Impulses and physiological states in theoretical models of nerve membrane," Biophys. J. **1**, 445–466 (1961).
[4] J.-I. Nagumo, S. Arimoto, and S. Yoshizawa, "An active pulse transmission line simulating nerve axon," Proc. IRE **50**, 2061–2070 (1962).
[5] E. M. Izhikevich, *Dynamical Systems in Neuroscience: The Geometry of Excitability and Bursting* (MIT Press, 2007).
[6] G. Russo and J.-J. E. Slotine, "Global convergence of quorum-sensing networks," Phys. Rev. E **82**, 041919 (2010).
[7] M. T. Schaub, N. O'Clery, Y. N. Billeh, J.-C. Delvenne, R. Lambiotte, and M. Barahona, "Graph partitions and cluster synchronization in networks of oscillators," Chaos **26**, 094821 (2016).
[8] F. Sorrentino, L. M. Pecora, A. M. Hagerstrom, T. E. Murphy, and R. Roy, "Complete characterization of the stability of cluster synchronization in complex dynamical networks," Sci. Adv. **2**, e1501737 (2016).
[9] E. Davison, B. Dey, and N. E. Leonard, "Synchronization bound for networks of nonlinear oscillators," in *Proceedings of the 54th Annual Allerton Conference on Communication, Control and Computing* (IEEE, 2016).
[10] Z. Aminzare, B. Dey, E. N. Davison, and N. E. Leonard, "Cluster synchronization of diffusively-coupled nonlinear systems: A contraction based approach," J. Nonlinear Sci. (published online).
[11] A. Hoff, J. V. d. Santos, C. Manchein, and H. A. Albuquerque, "Numerical bifurcation analysis of two coupled FitzHugh-Nagumo oscillators," Eur. Phys. J. B **87**, 151 (2014).
[12] S. A. Campbell and M. Waite, "Multistability in coupled FitzHugh-Nagumo oscillators," Nonlinear Anal. **47**, 1093–1104 (2001).
[13] É. Benoît, "Canards et enlacements," Publ. Math. Inst. Hautes Etudes Sci. **72**, 63–91 (1990).
[14] P. Szmolyan and M. Wechselberger, "Canards in $\mathbb{R}^3$," J. Differ. Equ. **177**, 419–453 (2001).
[15] C. Kuehn, *Multiple Time Scale Dynamics* (Springer, 2015), Vol. 191.
[16] M. Wechselberger, "Existence and bifurcation of canards in $\mathbb{R}^3$ in the case of a folded node," SIAM J. Appl. Dyn. Syst. **4**, 101–139 (2005).
[17] A. Milik, P. Szmolyan, H. Löffelmann, and E. Gröller, "Geometry of mixed-mode oscillations in the 3-D autocatalator," Int. J. Bifurcat. Chaos **8**, 505–519 (1998).
[18] É. Benoît, "Systemes lents-rapides dans $\mathbb{R}^3$ et leurs canards," Astérisque **109**, 159–191 (1983).
[19] K. Tchizawa, "On the two methods for finding 4-dimensional duck solutions," Appl. Math. **05**, 16 (2013).
[20] M. Wechselberger, "A propos de canards (apropos canards)," Trans. Am. Math. Soc. **364**, 3289–3309 (2012).
[21] M. Desroches, B. Krauskopf, and H. Osinga, "The geometry of slow manifolds near a folded node," SIAM J. Appl. Dyn. Syst. **7**, 1131–1162 (2008).
[22] M. Krupa and M. Wechselberger, "Local analysis near a folded saddle-node singularity," J. Differ. Equ. **248**, 2841–2888 (2010).
[23] R. Curtu and J. Rubin, "Interaction of canard and singular Hopf mechanisms in a neural model," SIAM J. Appl. Dyn. Syst. **10**, 1443–1479 (2011).
[24] M. Desroches, J. Guckenheimer, B. Krauskopf, C. Kuehn, H. M. Osinga, and M. Wechselberger, "Mixed-mode oscillations with multiple time scales," SIAM Rev. **54**, 211–288 (2012).
[25] V. Petrov, S. K. Scott, and K. Showalter, "Mixed-mode oscillations in chemical systems," J. Chem. Phys. **97**, 6191–6198 (1992).
[26] J. Moehlis, "Canards in a surface oxidation reaction," J. Nonlinear Sci. **12**, 319 (2002).
[27] J. Rubin and M. Wechselberger, "Giant squid-hidden canard: The 3D geometry of the Hodgkin–Huxley model," Biol. Cybern. **97**, 5–32 (2007).
[28] H. G. Rotstein, M. Wechselberger, and N. Kopell, "Canard induced mixed-mode oscillations in a medial entorhinal cortex layer II stellate cell model," SIAM J. Appl. Dyn. Syst. **7**, 1582–1611 (2008).
[29] M. Desroches, B. Krauskopf, and H. M. Osinga, "Mixed-mode oscillations and slow manifolds in the self-coupled FitzHugh-Nagumo system," Chaos **18**, 015107 (2008).
[30] K. Tchizawa and S. A. Campbell, "On winding duck solutions in $\mathbb{R}^4$," Proc. Neural Parallel Sci. Comput. **2**, 315–318 (2002).
[31] J.-M. Ginoux and J. Llibre, "Canards existence in FitzHugh-Nagumo and Hodgkin-Huxley neuronal models," Math. Prob. Eng. **2015**, 1 (2015).
[32] M. Krupa, B. Ambrosio, and M. Aziz-Alaoui, "Weakly coupled two-slow–two-fast systems, folded singularities and mixed mode oscillations," Nonlinearity **27**, 1555 (2014).
[33] M. G. Rosenblum, A. S. Pikovsky, and J. Kurths, "Phase synchronization of chaotic oscillators," Phys. Rev. Lett. **76**, 1804 (1996).
[34] B. van der Pol and J. van der Mark, LXXII. The heartbeat considered as a relaxation oscillation, and an electrical model of the heart," Lond. Edinb. Dubl. Phil. Mag. **6**, 763–775 (1928).
[35] L. Glass and R. Perez, "Fine structure of phase locking," Phys. Rev. Lett. **48**, 1772 (1982).
[36] M. R. Guevara, L. Glass, and A. Shrier, "Phase locking, period-doubling bifurcations, and irregular dynamics in periodically stimulated cardiac cells," Science **214**, 1350–1353 (1981).
[37] G. Matsumoto, K. Aihara, Y. Hanyu, N. Takahashi, S. Yoshizawa, J.-i. Nagumo, "Chaos and phase locking in normal squid axons," Phys. Lett. A **123**, 162–166 (1987).
[38] N. Kopell and G. Ermentrout, "Mechanisms of phase-locking and frequency control in pairs of coupled neural oscillators," Handb. Dyn. Syst. **2**, 3–54 (2002).
[39] U. Rutishauser, I. B. Ross, A. N. Mamelak, and E. M. Schuman, "Human memory strength is predicted by theta-frequency phase-locking of single neurons," Nature **464**, 903 (2010).
[40] X.-J. Wang, "Neurophysiological and computational principles of cortical rhythms in cognition," Physiol. Rev. **90**, 1195–1268 (2010).
[41] F. Varela, J.-P. Lachaux, E. Rodriguez, and J. Martinerie, "The brainweb: Phase synchronization and large-scale integration," Nat. Rev. Neurosci. **2**, 229 (2001).
[42] G. S. Medvedev and N. Kopell, "Synchronization and transient dynamics in the chains of electrically coupled FitzHugh–Nagumo oscillators," SIAM J. Appl. Math. **61**, 1762–1801 (2001).
[43] C. Rocsoreanu, A. Georgescu, and N. Giurgiteanu, *The FitzHugh-Nagumo Model: Bifurcation and Dynamics* (Springer Science & Business Media, 2012), Vol. 10.
[44] J. Rinzel, "Models in neurobiology," in *Nonlinear Phenomena in Physics and Biology*, edited by R. H. Enns, B. L. Jones, R. M. Miura, and S. S. Rangnekar (Springer New York, Boston, MA, 1981), pp. 345–367.
[45] M. Brøns, "Excitation and annihilation in the FitzHugh-Nagumo equations," IMACS Trans. Sci. Comp. **1**, 297–301 (1989).
[46] J. Guckenheimer and P. Holmes, *Nonlinear Oscillations, Dynamical Systems, and Bifurcations of Vector Fields* (Springer Science & Business Media, 2013), Vol. 42.
[47] J. Moehlis, "Canards for a reduction of the Hodgkin-Huxley equations," J. Math. Biol. **52**, 141–153 (2006).
[48] A. Dhooge, W. Govaerts, and Y. A. Kuznetsov, "MATCONT: A MATLAB package for numerical bifurcation analysis of ODEs," ACM Trans. Math. Softw. (TOMS) **29**, 141–164 (2003).

[49] P. Eckhoff and P. Holmes, *A Short Course in Mathematical Neuroscience*, course notes, Princeton University, Fall 2006.
[50] B. Hassard and Y. Wan, "Bifurcation formulae derived from center manifold theory," J. Math. Anal. Appl. **63**, 297–312 (1978).
[51] S. M. Baer and T. Erneux, "Singular Hopf bifurcation to relaxation oscillations," SIAM J. Appl. Math. **46**, 721–739 (1986).
[52] J. Rinzel and J. P. Keaner, "Hopf bifurcation to repetitive activity in nerve," SIAM J. Appl. Math. **43**, 907–922 (1983).
[53] M. Brøns,"Relaxation oscillations and canards in a nonlinear model of discontinuous plastic deformation in metals at very low temperatures," in *Proceedings of the Royal Society of London A: Mathematical, Physical and Engineering Sciences* (The Royal Society, 2005), Vol. 461, pp. 2289–2302.
[54] G. Russo and J. J. E. Slotine, "Global convergence of quorum-sensing networks," Phys. Rev. E **82**, 041919 (2010).
[55] M. Wechselberger, J. Mitry, and J. Rinzel, "Canard theory and excitability," in *Nonautonomous Dynamical Systems in the Life Sciences*, Lecture Notes in Mathematics Vol. 2102, edited by P. E. Kloeden and C. Pötzsche (Springer International Publishing, 2013).
[56] F. Takens, "Unfoldings of certain singularities of vectorfields: Generalized Hopf bifurcations," J. Differ. Equ. **14**, 476–493 (1973).
[57] M. Golubitsky and W. F. Langford, "Classification and unfoldings of degenerate Hopf bifurcations," J. Differ. Equ. **41**, 375–415 (1981).
[58] M. Brøns, M. Krupa, and M. Wechselberger, "Mixed mode oscillations due to the generalized canard phenomenon," Fields Inst. Commun. **49**, 39–63 (2006).
[59] C. Perryman and S. Wieczorek, "Adapting to a changing environment: Non-obvious thresholds in multi-scale systems," Proc. R. Soc. Lond. A Math. Phys. Eng. Sci. **470**, 20140226 (2014).